RESTRICTED

Copy No. 133
RM No. L8L31a

NACA

RESEARCH MEMORANDUM

EFFECT OF AIRFOIL PROFILE OF SYMMETRICAL SECTIONS ON THE LOW-SPEED ROLLING DERIVATIVES OF 45° SWEPTBACK-WING MODELS OF ASPECT RATIO 2.61

By

William Letko and Jack D. Brewer

Langley Aeronautical Laboratory
Langley Air Force Base, Va.

NATIONAL ADVISORY COMMITTEE
FOR AERONAUTICS

WASHINGTON

March 4, 1949

RESTRICTED

NATIONAL ADVISORY COMMITTEE FOR AERONAUTICS

RESEARCH MEMORANDUM

EFFECT OF AIRFOIL PROFILE OF SYMMETRICAL SECTIONS ON THE LOW-SPEED ROLLING DERIVATIVES OF 45° SWEPTBACK-WING MODELS OF ASPECT RATIO 2.61

By William Letko and Jack D. Brewer

SUMMARY

An investigation was made in the Langley stability tunnel to determine the effect of airfoil profile of symmetrical sections on the rolling derivatives of three untapered wings having 45° sweepback. The wings had the following profiles normal to the leading edge: biconvex (12 percent thick), NACA 65_1-012, and NACA 0012. The aspect ratio for each wing was 2.61.

Calculations were made to determine the effect of different wing profiles on the stability boundaries and motions at subsonic speeds of a typical transonic airplane configuration.

Results of the tests indicate that increasing the sharpness of the leading edge of the airfoil decreased the range of lift coefficients over which the derivatives maintained their initial trends and usually decreased the maximum values of the derivatives obtained in the unstalled range.

In general, the effect on the derivatives of adding a leading-edge spoiler to the inboard half of the NACA 0012 wing appeared to be equivalent to increasing the sharpness of the entire leading edge to some value between that of the NACA 0012 wing profile and the NACA 65_1-012 wing profile.

Results of the calculations of the dynamic stability of a typical transonic airplane configuration showed that at 0.2 lift coefficient, changes in airfoil profile had only a small effect on the oscillatory and spiral stability boundaries of a typical transonic airplane configuration. At higher lift coefficients (0.5 and 0.8), increases in the sharpness of the leading edge usually caused a stabilizing shift of both the oscillatory and spiral stability boundaries. The stabilizing shift in the spiral stability boundary was more than compensated for, however, by the changes in effective dihedral of the airplane wings. An increased sharpness of the leading edge therefore caused an increased tendency toward spiral instability, particularly at the higher lift coefficients.

INTRODUCTION

Estimation of dynamic flight characteristics of aircraft requires a knowledge of the forces and moments resulting from the angular motions of the airplane. The relationship between the forces and moments and the angular motions are commonly expressed in nondimensional terms known as the rotary derivatives. In the past, these derivatives have generally been estimated from theory because of the lack of a convenient experimental technique.

The recent application of the rolling-flow and curved-flow principles of the Langley stability tunnel (references 1 and 2), however, has made the determination of the rotary derivatives relatively simple. A systematic research program utilizing these new experimental techniques has been established to determine the effects of various geometric variables on rotary and static stability characteristics.

The present investigation was made to determine the effects of airfoil profile of symmetrical sections on the low-speed static stability and rolling characteristics of sweptback wings. One wing, having a blunt leading edge, (NACA 0012 airfoil section) was tested with and without a leading-edge spoiler extending from the plane of symmetry to the 50-percent semispan point of each wing panel to determine whether there might be an advantage in a wing having a section varying from sharp nose at the wing root to round nose at the wing tip. Results of tests to determine the static- and yawing-stability derivatives of the wings used in the present investigation are reported in reference 3.

Motions and stability boundaries, calculated by using the stability derivatives obtained from the data of this paper and from those of references 2 to 4, are also included in this paper. These results are presented to show the effect of changes of the wing section on the stability characteristics at subsonic speeds of a typical transonic airplane configuration such as that of references 2 and 4.

SYMBOLS

The results of the tests are presented as standard NACA coefficients of forces and moments which are referred to the stability axes with the origin at the quarter-chord point of the mean aerodynamic chord of the models tested. The positive directions of the forces, moments, and angular displacements are shown in figure 1. The system of axes and angular relationships used in calculating the stability boundaries and motions are shown in figure 2.

The coefficients and symbols used herein are defined as follows:

V free-stream velocity (also, velocity of airplane), feet per second

v airplane sideslip velocity (positive sideslip to the right), feet per second

ρ mass density of air, slugs per cubic foot

q dynamic pressure, pounds per square foot $\left(\frac{1}{2}\rho V^2\right)$

S wing area, square feet

b wing span, measured perpendicular to plane of symmetry, feet

A aspect ratio $\left(b^2/S\right)$

c chord of wing measured parallel to axis of symmetry, feet

$\bar{c}$ mean aerodynamic chord, feet $\left(\frac{2}{S}\int_0^{b/2} c^2 dy\right)$

x distance of quarter-chord point of any chordwise section from leading edge of root section, feet

$\bar{x}$ distance of quarter chord of mean aerodynamic chord from leading edge of root chord, feet $\left(\frac{2}{S}\int_0^{b/2} cx\, dy\right)$

y spanwise distance measured perpendicular to axis of symmetry, feet

W weight of airplane, pounds

m mass, slugs $\left(W/g\right)$

g acceleration due to gravity, feet per second per second

μ relative-density factor $\left(m/\rho Sb\right)$

k_{X_o} radius of gyration about principal longitudinal axis, feet

k_{Z_o} radius of gyration about principal vertical axis, feet

K_X nondimensional radius of gyration about longitudinal stability axis $\left(\sqrt{\left(\frac{k_{X_o}}{b}\right)^2 \cos^2\eta + \left(\frac{k_{Z_o}}{b}\right)^2 \sin^2\eta}\right)$

K_Z nondimensional radius of gyration about vertical stability axis $\left(\sqrt{\left(\frac{k_{Z_o}}{b}\right)^2 \cos^2\eta + \left(\frac{k_{X_o}}{b}\right)^2 \sin^2\eta}\right)$

K_{XZ} nondimensional product-of-inertia parameter $\left(\sqrt{\left[\left(\frac{k_{Z_o}}{b}\right)^2 - \left(\frac{k_{X_o}}{b}\right)^2\right] \cos\eta \sin\eta}\right)$

C_L lift coefficient (L/qS)

C_D drag coefficient $\left(-C_X \text{ for } \psi = 0^\circ\right)$

C_X longitudinal-force coefficient (X/qS)

C_Y lateral-force coefficient (Y/qS)

C_l rolling-moment coefficient (L'/qSb)

C_m pitching-moment coefficient ($M/qS\bar{c}$)

C_n yawing-moment coefficient (N/qSb)

L lift, pounds

X longitudinal force, pounds

Y lateral force, pounds

L' rolling moment about X-axis, foot-pounds

M pitching moment about Y-axis, foot-pounds

N yawing moment about Z-axis, foot-pounds

α angle of attack, measured in plane of symmetry (also angle between reference axis and flight-path axis), degrees

ψ angle of yaw, degrees

Λ angle of sweepback, degrees

β angle of sideslip, radians, $\left(\tan^{-1}\frac{v}{V}\right)$

η angle of attack of principal longitudinal axis of airplane, positive when principal axis is above flight path, degrees (see fig. 2)

γ angle of flight path with respect to horizontal, positive when flight-path axis is above horizontal axis, degrees (see fig. 2)

ϵ angle between reference axis and principal axis, positive when reference axis is above principal axis, degrees (see fig. 2)

t time, seconds

R Routh's discriminant

$\frac{pb}{2V}$ wing-tip helix angle, radians

p rolling angular velocity, radians per second

$\frac{rb}{2V}$ yawing-velocity parameter

r yawing angular velocity, radians per second

$$C_{Y_\beta} = \frac{\partial C_Y}{\partial \beta}$$

$$C_{n_\beta} = \frac{\partial C_n}{\partial \beta}$$

$$C_{l_\beta} = \frac{\partial C_l}{\partial \beta}$$

$$C_{Y_p} = \frac{\partial C_Y}{\partial\left(\frac{pb}{2V}\right)}$$

$$C_{n_p} = \frac{\partial C_n}{\partial\left(\frac{pb}{2V}\right)}$$

$$C_{l_p} = \frac{\partial C_l}{\partial\left(\frac{pb}{2V}\right)}$$

$$C_{Y_r} = \frac{\partial C_Y}{\partial\left(\frac{rb}{2V}\right)}$$

$$C_{n_r} = \frac{\partial C_n}{\partial\left(\frac{rb}{2V}\right)}$$

$$C_{l_r} = \frac{\partial C_l}{\partial\left(\frac{rb}{2V}\right)}$$

APPARATUS AND TEST

The present investigation was conducted in the 6-foot circular test section of the Langley stability tunnel. This section is equipped with a motor-driven rotor which imparts a twist to the air stream so that a model mounted in the tunnel is in a field of flow similar to that which exists about an airplane in rolling flight (reference 1).

The models tested consisted of three untapered wings of 45° sweepback and aspect ratio 2.61. The models had the following profiles in planes normal to the leading edge: biconvex (12 percent thick), NACA 65_1-012, and NACA 0012. The plan form of the models and the three profiles are shown in figure 3. Also shown in figure 3 is the semispan leading-edge spoiler which, for some tests, was mounted on the wing with the NACA 0012 section.

All tests were made with the model mounted rigidly at the quarter-chord point of the mean aerodynamic chord on a single-strut support as shown in figure 4. The forces and moments were measured by means of electrical strain gages contained in the strut. The dynamic pressure at which the tests were made was approximately 39.7 pounds per square foot which corresponds to a Mach number of 0.17. The Reynolds number based on the mean aerodynamic chord of the models was 1,400,000.

The models were tested through an angle-of-attack range from about -2° angle of attack up to and beyond the angle of maximum lift in straight flow at 0° angle of yaw and in rolling flow at values of $pb/2V$ of ± 0.021 and ± 0.062. In straight flow, six-component measurements were made, whereas only measurements of lateral force, yawing moment, and rolling moment were obtained in rolling flow.

CORRECTIONS

Approximate corrections, similar to those of reference 5, based on unswept-wing theory, for the effects of jet boundaries have been applied to the angle of attack, the longitudinal-force coefficient, and the rolling-moment coefficient. Corrections for blocking or turbulence have not been applied to the results.

RESULTS AND DISCUSSION

Characteristics in Straight Flow

The lift, longitudinal-force, and pitching-moment characteristics as measured in straight flow are presented in figure 5. These results are about the same as those of reference 3 which were obtained at a dynamic pressure of 24.9 pounds per square foot. As was pointed out in reference 3, the lowest lift-curve slope at low lift coefficients was obtained with the biconvex section; and the highest maximum lift was obtained with the NACA 0012 wing equipped with the inboard leading-edge spoiler. Effectively increasing the sharpness of the leading edge reduced the rearward shift of the aerodynamic center with lift coefficient.

Characteristics in Rolling Flow

As can be seen from figure 6, increasing the sharpness of the leading edge decreased the maximum positive value of C_{Y_p} and decreased the range of lift coefficients over which the variation of C_{Y_p} with lift coefficient remained linear. The values of C_{n_p} at low and medium lift coefficients are small and negative and are little affected by airfoil profile. However, increasing the sharpness of the leading edge of the airfoil decreased the maximum negative values of C_{n_p} and decreased

the lift coefficient at which the values of C_{n_p} became positive. For certain airplane configurations having a high vertical tail, it might be possible that C_{n_p} would be positive throughout the lift coefficient range, which would be of importance from the viewpoint of stability and control. The biconvex wing had the lowest value of C_{l_p} at low lift coefficients. This might be expected since the biconvex wing has the lowest lift-curve slope at low lift coefficients. As with C_{Y_p} and C_{n_p}, increasing the sharpness of the leading edge of the wing decreased the lift coefficient at which large changes generally occurred in the initial trends of the variation of C_{l_p} with lift coefficient.

In general, the effect on the derivatives, especially on C_{Y_p} and C_{n_p}, of adding the leading-edge spoiler to the NACA 0012 airfoil appeared to be equivalent to increasing effectively the sharpness of the leading edge to some value between that of the NACA 0012 airfoil and that of the NACA 65_1-012 airfoil.

Drag Increment, $C_D - \frac{C_L^2}{\pi A}$

It was pointed out in reference 3 that the increment of drag that is not associated with lift $\left(C_D - \frac{C_L^2}{\pi A}\right)$ could be used to indicate the lift coefficient at which separation begins to take place on plain wings. It was shown that large changes in certain aerodynamic characteristics may occur at the lift coefficient at which this drag increment begins to rise. A plot of $C_D - \frac{C_L^2}{\pi A}$ against lift coefficient for the wings tested is presented in figure 7. It can be seen by comparing this figure with figure 6 that abrupt changes in the initial trends of C_{Y_p}, C_{n_p}, and C_{l_p} generally do occur at approximately the same lift coefficient at which the drag increment begins to increase. This lift coefficient is about 0.6 for the NACA 0012 wing, about 0.4 for the NACA 65_1-012 wing, and 0.3 for the biconvex wing. Ordinarily, changes in the drag increment can be expected to be useful only for predicting changes in the characteristics of plain wings. However, the increase in the drag increment for the wing with the inboard nose spoiler occurs at about 0.4 lift coefficient, at which lift coefficient the aerodynamic characteristics also change

abruptly. As was pointed out in reference 3, the relationship between the drag increment and the extent of linearity of the stability derivatives might serve as a basis for making certain qualitative estimates of the effects of Reynolds number on the stability derivatives when only the lift and drag variations with Reynolds number have been determined.

Stability Boundaries and Motions

Computations were made to determine the changes in the stability boundaries and in the motions of an airplane caused by changes in the stability derivatives resulting from using wings of different profile. The geometric and mass characteristics of the airplane remained the same in each case, and the stability derivatives of the airplane differed only by the different contribution of the wing profile used in combination with the airplane.

The airplane configuration used, shown in figure 8, is similiar to the model used in references 2 and 4 and the contribution of the fuselage and tail to the stability derivatives was obtained from the data of these references. The contributions of the different wings to the stability derivatives were obtained from results of the present tests and from tests of reference 3. The mass characteristics assumed were those of a typical transonic airplane.

The stability derivatives and mass characteristics used in the computations are given in tables I and II. The boundaries and motions were calculated by means of the equations listed in reference 6.

In figure 9 are presented the oscillatory and spiral stability boundaries as functions of C_{n_β} and C_{l_β} for the three airplanes which differ only in wing profile. From the figure, it can be seen that the effect of airplane wing profile on both the oscillatory and spiral stability boundaries is comparatively small at a lift coefficient of 0.2. At the higher lift coefficients there are much larger effects of airfoil section on both boundaries. At lift coefficients of 0.5 and 0.8 there is a stabilizing shift of the spiral stability boundary as the sharpness of the leading edge is increased. At 0.5 lift coefficient there is a large stabilizing shift in the oscillatory boundary when changing from the NACA 0012 wing to either of the other sections which have sharper leading edges. There is little difference, however, in the oscillatory boundaries obtained for the NACA 65_1-012 and the biconvex wings. At 0.8 lift coefficient there is a progressive stabilizing shift of the oscillatory stability boundary as well as the spiral stability boundary as the sharpness of the leading edge is increased.

The stability boundaries are presented in figure 10 with a point to show the position of the particular airplane configuration with respect to the boundaries. At a lift coefficient of 0.2 oscillatory instability is indicated for all the airplane configurations. The large stabilizing shift of the oscillatory boundaries resulting from a change of lift coefficient from 0.2 to 0.5 is mainly caused by the change in η, the inclination of the principal longitudinal axis with respect to the flight path, from about -3° at 0.2 lift coefficient to about 2.5° at 0.5 lift coefficient. Reference 6 indicates that the inclination of the principal longitudinal axis above the flight path generally causes a stabilizing shift of the oscillatory boundary while an inclination below the flight path results in a destabilizing shift of the oscillatory boundary. At a lift coefficient of 0.5 all the airplane configurations fall in the stable region. As the sharpness of the leading edge of the wing increases, the position of the airplane becomes closer to the spiral stability boundary. At a lift coefficient of 0.8, there is a shift in position of the airplane into the spiral divergence region with an increase in sharpness of the wing leading edge; the airplane with NACA 0012 wing falls in the stable region, the airplane with the NACA 65_1-012 wing falls in the spiral divergence region near the spiral stability boundary, and the airplane with the wing of biconvex section falls well in the spiral divergence region. It should be noted that although increases in the sharpness of the leading edge of the wings generally affect the derivatives in such a way as to cause a stabilizing shift in the stability boundaries, there is at the same time a detrimental effect on C_{l_β} from the standpoint of spiral stability.

The motions in bank and sideslip due to a small initial angle of sideslip for each of the airplane configurations is shown in figure 11 for a lift coefficient of 0.8. The motions are presented as angles of sideslip or bank, relative to the initial sideslip angle, and should be reliable provided the sideslip angle does not exceed that at which the derivatives become nonlinear. The airplane with the biconvex section shows extreme spiral divergence, the angle of sideslip increasing and the airplane banking rapidly in the direction of sideslip to excessive values of both sideslip and bank. The airplane with the NACA 65_1-012 wing is slightly spirally unstable, banking to only a small angle in the first second, but the amplitude of the oscillation increases with time. Slight spiral instability is not considered serious from the standpoint of control.

The airplane with the NACA 0012 wing falls in the stable region of the stability diagram (as can be seen in fig. 10) and the motion in bank and sideslip is stable. Although the motion in bank is stable, the airplane attains a relatively high angle of bank in the first second and a

half. In about four and a half seconds, the amplitude decreases to less than one-quarter of the maximum value.

It should be mentioned that the derivatives used in calculating the boundaries and motions are those obtained from tests at low Reynolds numbers. Although airfoil section effects similar to those described would still occur at a higher Reynolds number they might not be important at as low lift coefficients, since, at higher Reynolds numbers, the derivatives obtained for the wings might continue their initial linear trends to higher lift coefficients. This would alter considerably the boundaries and motions at 0.8 lift coefficient and would probably cause an appreciable change in the boundaries and motions for 0.5 lift coefficient. Calculations (not presented) of the boundaries were made using straight-line extrapolations of the data for the NACA 0012 wing for a lift coefficient of 0.8. The results showed a stabilizing shift of the oscillatory boundary and a destabilizing shift of the spiral stability boundary. The position of the airplane with the NACA 0012 wing was shifted up and to the right in the stability diagram (C_{l_β} becoming more negative and C_{n_β} more positive) and it appears that similar extrapolations of the curves for the NACA 65_1-012 and biconvex wings would at least give negative values of C_{l_β} and might shift the airplanes having these wing sections into the stable region (even though there might be a concurrent destabilizing shift of the spiral boundary).

CONCLUSIONS

The results of low-scale tests made to determine the effect of airfoil profile of symmetrical sections on the low-speed rolling stability derivatives of untapered 45° sweptback-wing models of aspect ratio 2.61, and the results of calculations made to determine the effect on the dynamic stability at subsonic speeds of a transonic airplane configuration using the different wing profiles indicate the following conclusions:

1. Increasing the sharpness of the leading edge of the airfoil decreased the range of lift coefficients over which the rolling derivatives maintained their initial trends and usually decreased the maximum values of the derivatives obtained in the unstalled range.

2. In general, the effect on the rolling derivatives of adding an inboard leading-edge spoiler to the NACA 0012 airfoil appeared to be equivalent to increasing effectively the sharpness of the entire leading edge to some value between that of the NACA 0012 section and that of the NACA 65_1-012 section.

3. Changes in airfoil section had only a small effect on the oscillatory and spiral stability boundaries of a typical transonic airplane configuration at 0.2 lift coefficient. At higher lift coefficients (0.5 and 0.8) increases in leading-edge sharpness usually caused a stabilizing shift in both the oscillatory and spiral stability boundaries. The stabilizing shift in the spiral stability boundary was more than compensated for, however, by the changes in effective dihedral of the wings. An increased sharpness of the leading edge, therefore, caused an increased tendency toward spiral instability, particularly at the higher lift coefficients.

Langley Aeronautical Laboratory
National Advisory Committee for Aeronautics
Langley Air Force Base, Va.

REFERENCES

1. MacLachlan, Robert, and Letko, William: Correlation of Two Experimental Methods of Determining the Rolling Characteristics of Unswept Wings. NACA TN No. 1309, 1947.

2. Bird, John D., Jaquet, Byron M., and Cowan, John: Effect of Fuselage and Tail Surfaces on Low-Speed Yawing Characteristics of a Swept-Wing Model as Determined in Curved-Flow Test Section of Langley Stability Tunnel. NACA RM No. L8G13, 1948.

3. Letko, William, and Jaquet, Byron M.: Effect of Airfoil Profile of Symmetrical Sections on the Low-Speed Static-Stability and Yawing Derivatives of 45° Sweptback Wing Models of Aspect Ratio 2.61. NACA RM No. L8H10, 1948.

4. Bird, John D., Lichtenstein, Jacob H., and Jaquet, Byron M., Investigation of the Influence of Fuselage and Tail Surfaces on Low-Speed Static Stability and Rolling Characteristics of a Swept-Wing Model. NACA RM No. L7H15, 1947.

5. Feigenbaum, David, and Goodman, Alex: Preliminary Investigation at Low Speeds of Swept Wings in Rolling Flow. NACA RM No. L7E09, 1947.

6. Sternfield, Leonard: Effect of Product of Inertia on Lateral Stability. NACA TN No. 1193, 1947.

TABLE I

GEOMETRIC AND MASS CHARACTERISTICS

USED IN STABILITY CALCULATIONS

C_L	0.2	0.5	0.8
W, lb	11250	11250	11250
S, sq ft	352	352	352
b, ft	30.4	30.4	30.4
p, slugs/cu ft	0.001266	0.001266	0.001266
V, ft/sec	499	316	250
μ	25.8	25.8	25.8
k_{X_o}, ft	2.875	2.875	2.875
k_{Z_o}, ft	9.391	9.391	9.391
K_x^2	0.00918	0.00913	0.01054
K_z^2	0.09514	0.09523	0.09385
K_{xz}^2	-0.00470	0.00395	0.01163
α, deg	3.88	9.65	14.82
η, deg	α - 7	α - 7	α - 7
γ, deg	0	0	0

TABLE II

STABILITY DERIVATIVES USED TO CALCULATE LATERAL-STABILITY BOUNDARIES

	Airplane with NACA 0012 wing			Airplane with NACA 65_1-012 wing			Airplane with biconvex wing		
C_L, tail off	0.2	0.5	0.8	0.2	0.5	0.8	0.2	0.5	0.8
C_{n_r}, tail off	-.049	-.051	-.051	-.053	-.035	-.038	-.043	-.030	-.038
C_{l_r}, tail off	.080	.216	.229	.070	.124	.050	.055	.042	-.049
C_{n_p}, tail off	-.016	-.064	.116	-.002	.036	.055	-.002	.046	.052
C_{l_p}, tail off	-.222	-.246	-.400	-.220	-.305	-.297	-.217	-.325	-.240
C_{Y_β}, tail off	-.094	-.085	.033	-.095	-.059	-.202	-.095	-.095	-.213
C_{n_β}, tail off	-.037	-.024	-.061	-.042	-.038	-.036	-.045	-.038	-.048
Derivatives used to calculate lateral motions									
C_{Y_r}			0.077			0.464			0.383
C_{n_r}			-.192			-.179			-.179
C_{l_r}			.211			.032			-.067
C_{Y_p}			.272			.225			.225
C_{n_p}			.043			-.018			-.021
C_{l_p}			-.390			-.287			-.230
C_{Y_β}			-.180			-.386			-.397
C_{n_β}			.049			.075			.063
C_{l_β}			-.151			.004			.108

NACA

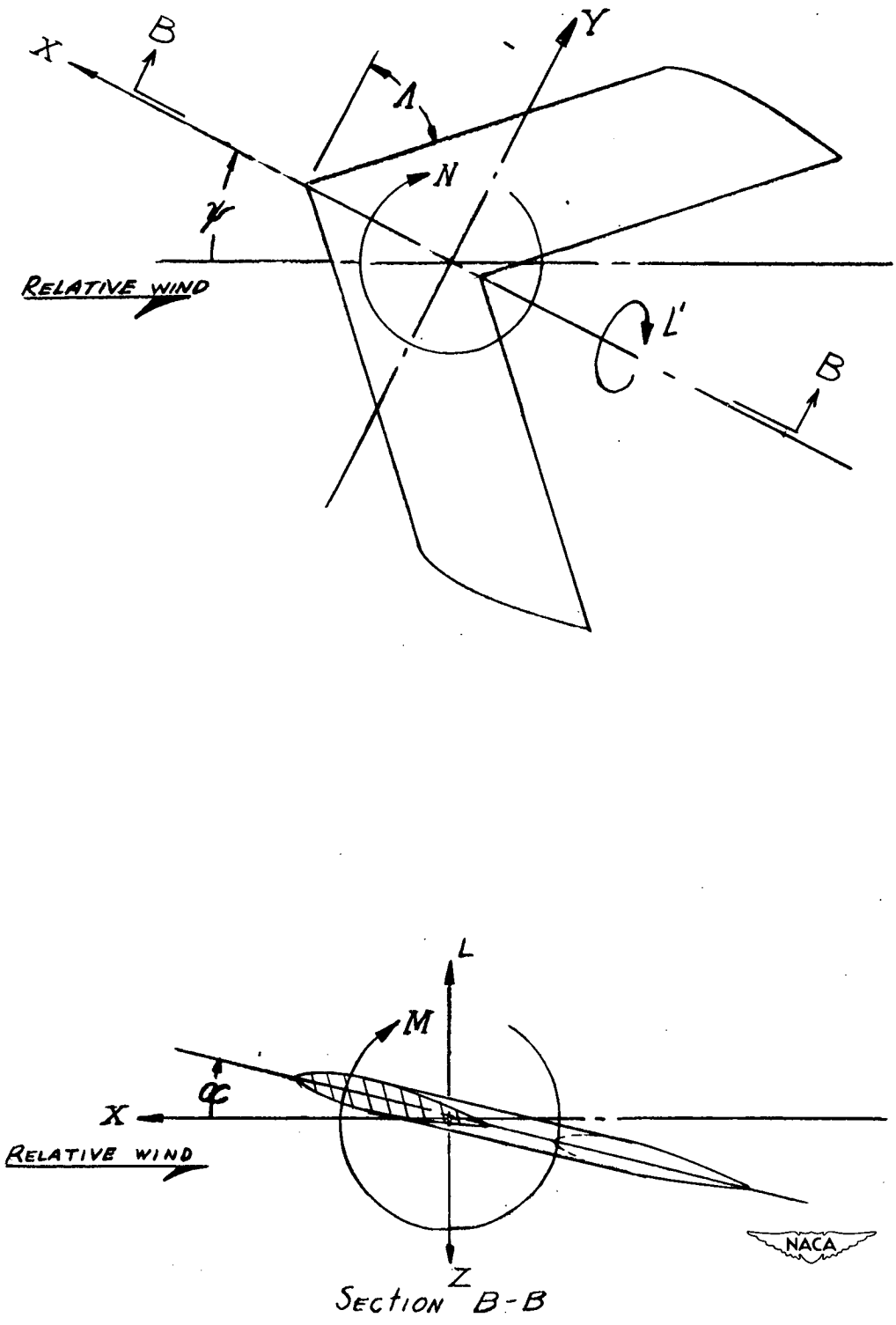

Figure 1.– System of axes used. Positive directions of forces, moments, and angles are indicated.

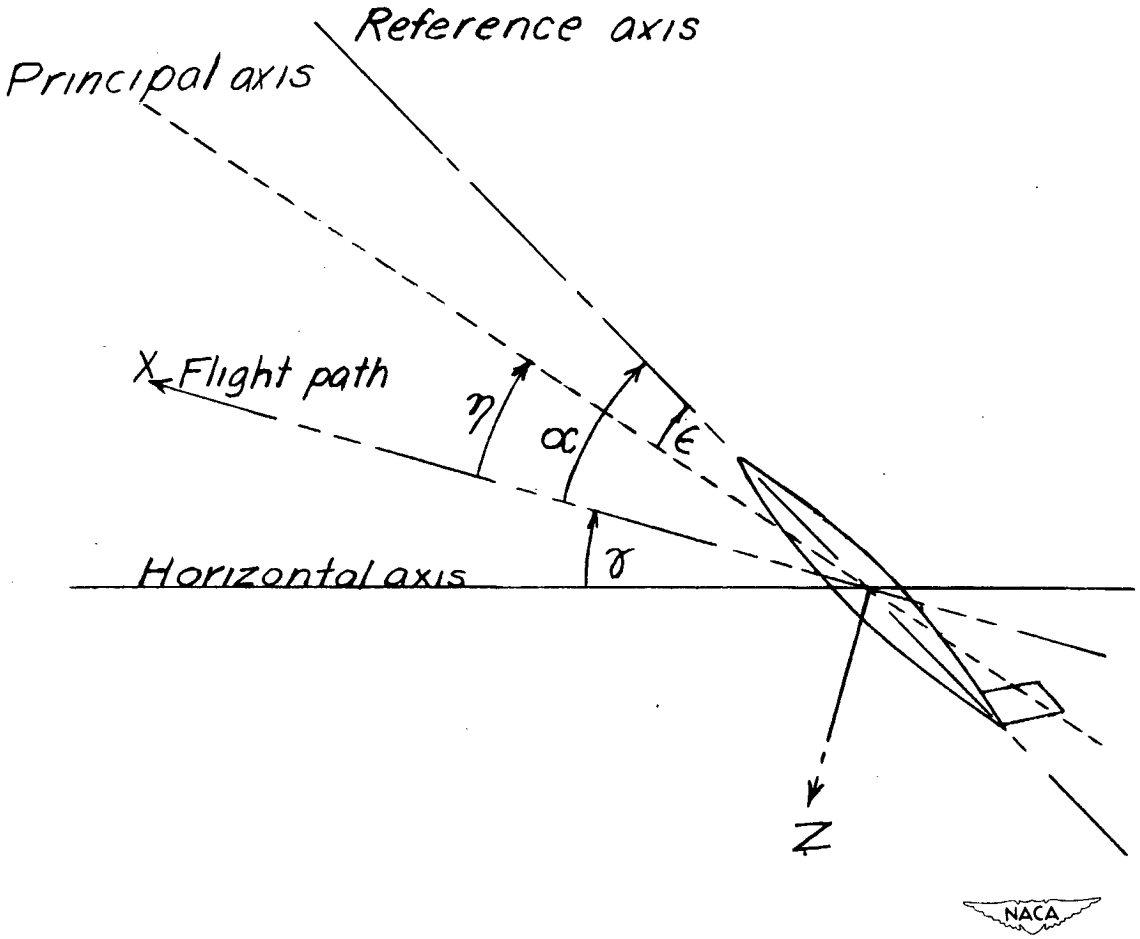

Figure 2.– System of axes and angular relationships used in calculations of stability boundaries and motions. $\eta = \alpha - \epsilon$.

Page intentionally left blank

18, 20,

Page intentionally left blank

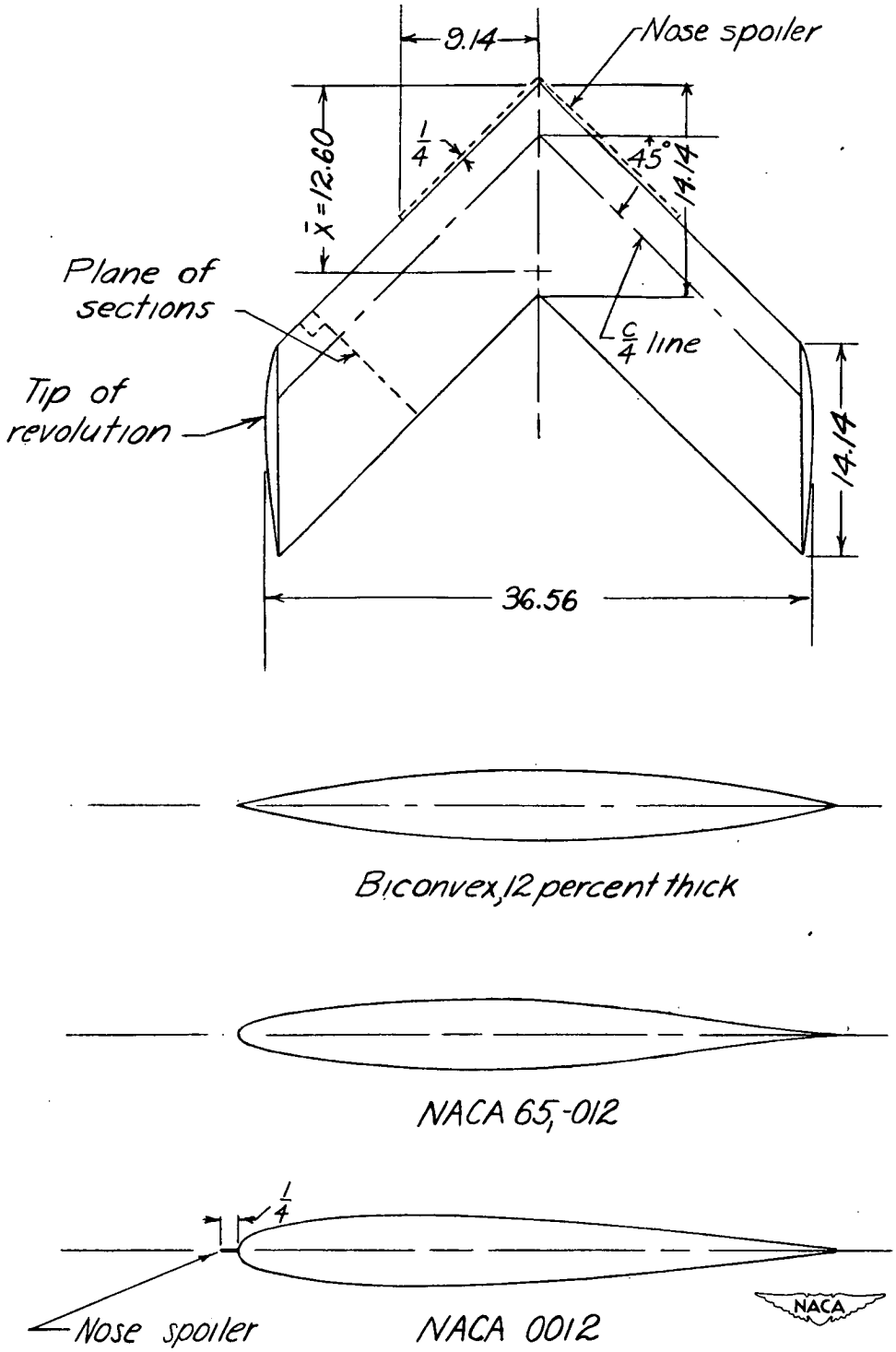

Figure 3.- Sketch of the plan form and airfoil profiles of the models investigated. All dimensions are in inches. Wing area equals 3.56 square feet.

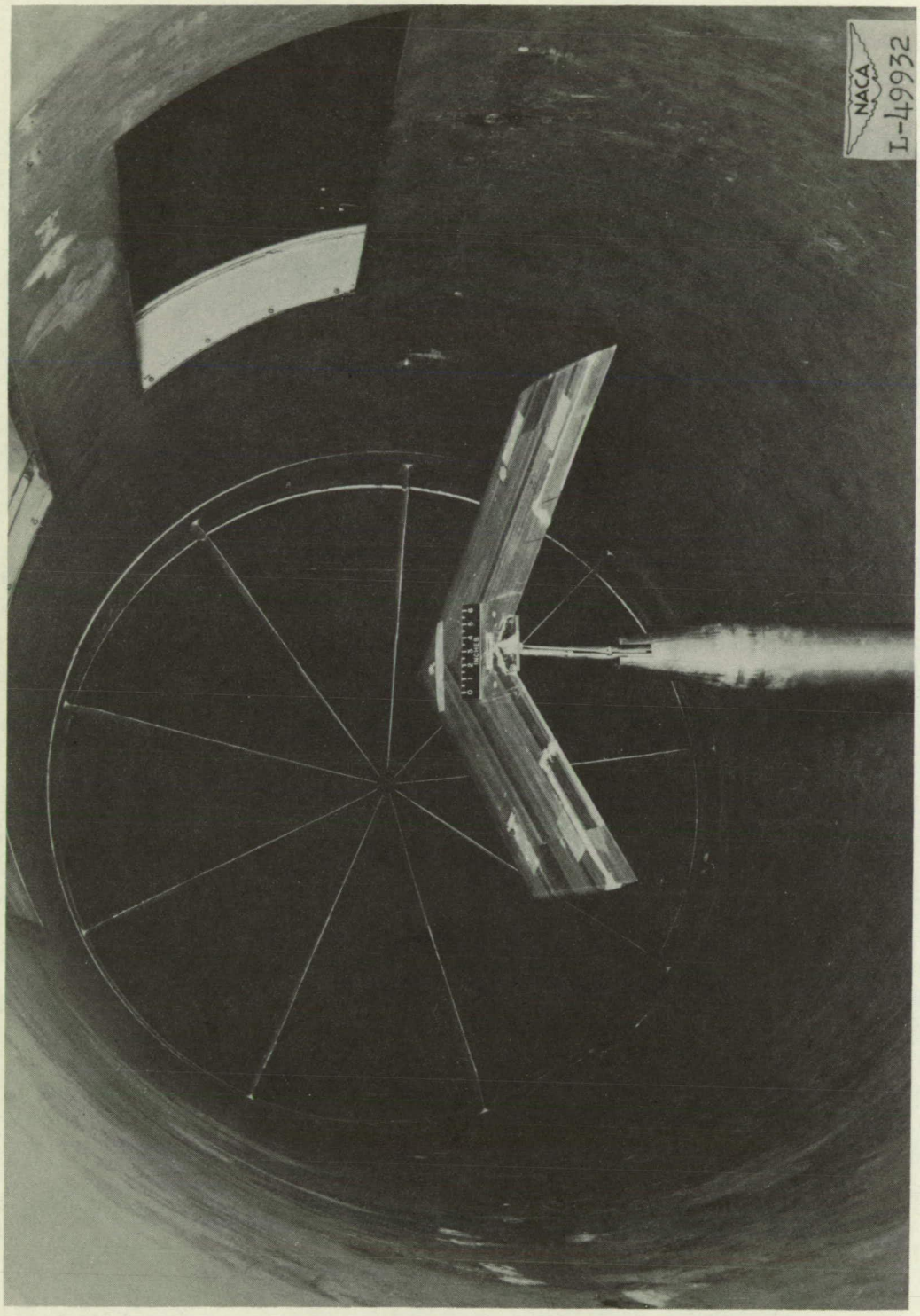

Figure 4.- The 45° sweptback wing mounted in the rolling-flow test section of the Langley stability tunnel. NACA 0012 airfoil section.

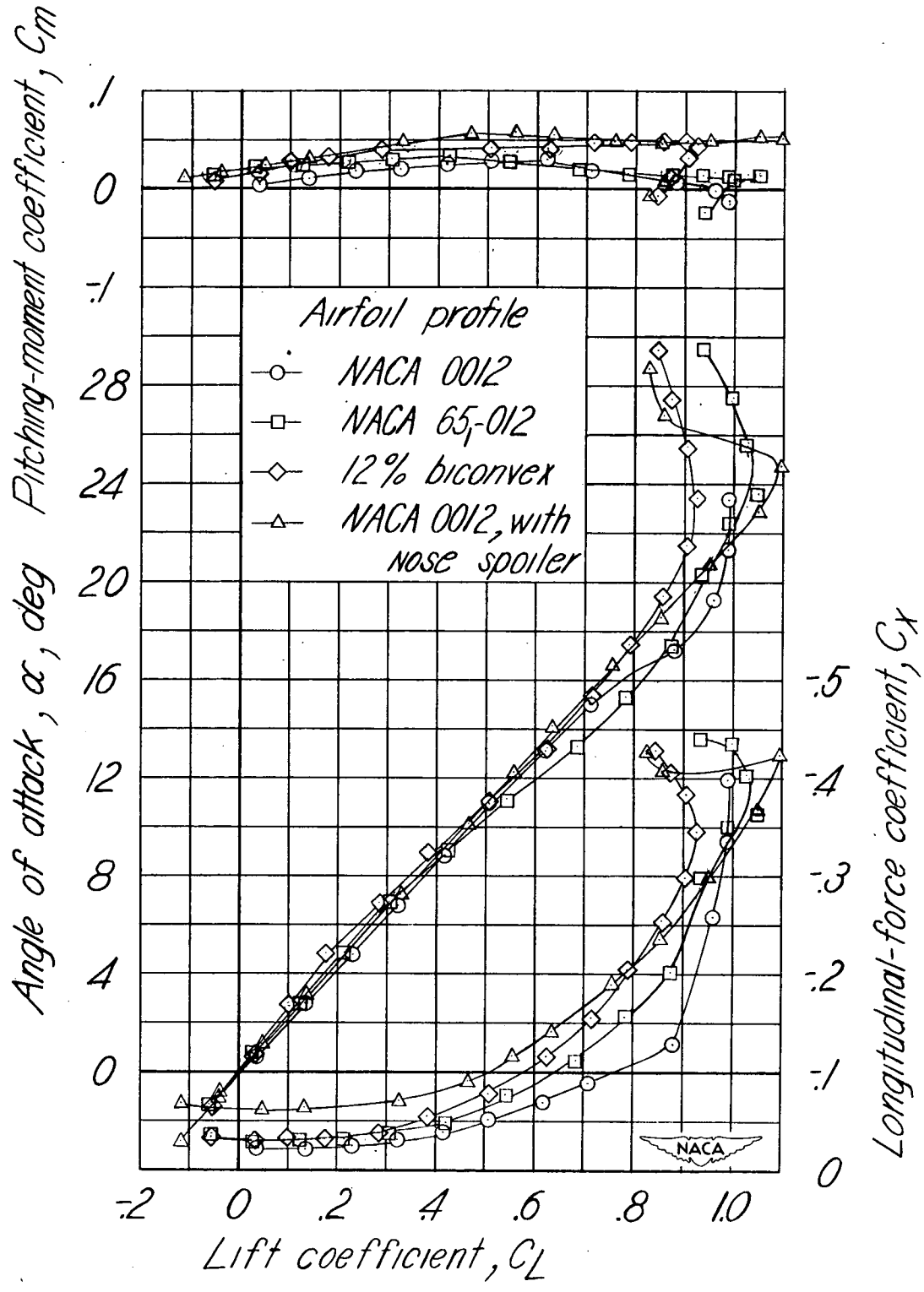

Figure 5.- Variation of C_m, C_x, and α with lift coefficient for the wings tested.

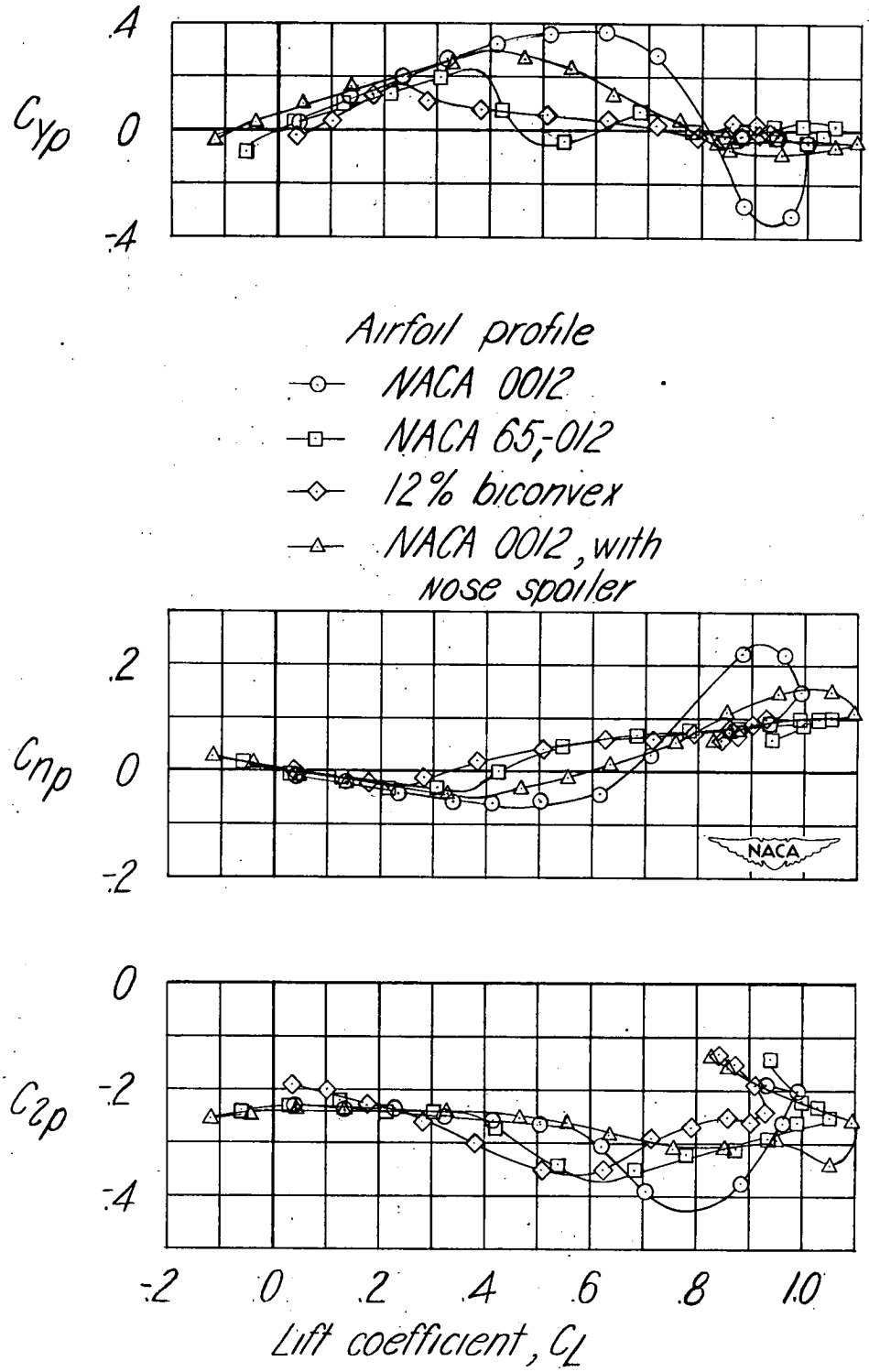

Figure 6.– Variations of C_{y_p}, C_{n_p}, and C_{l_p} with lift coefficient for the wings tested.

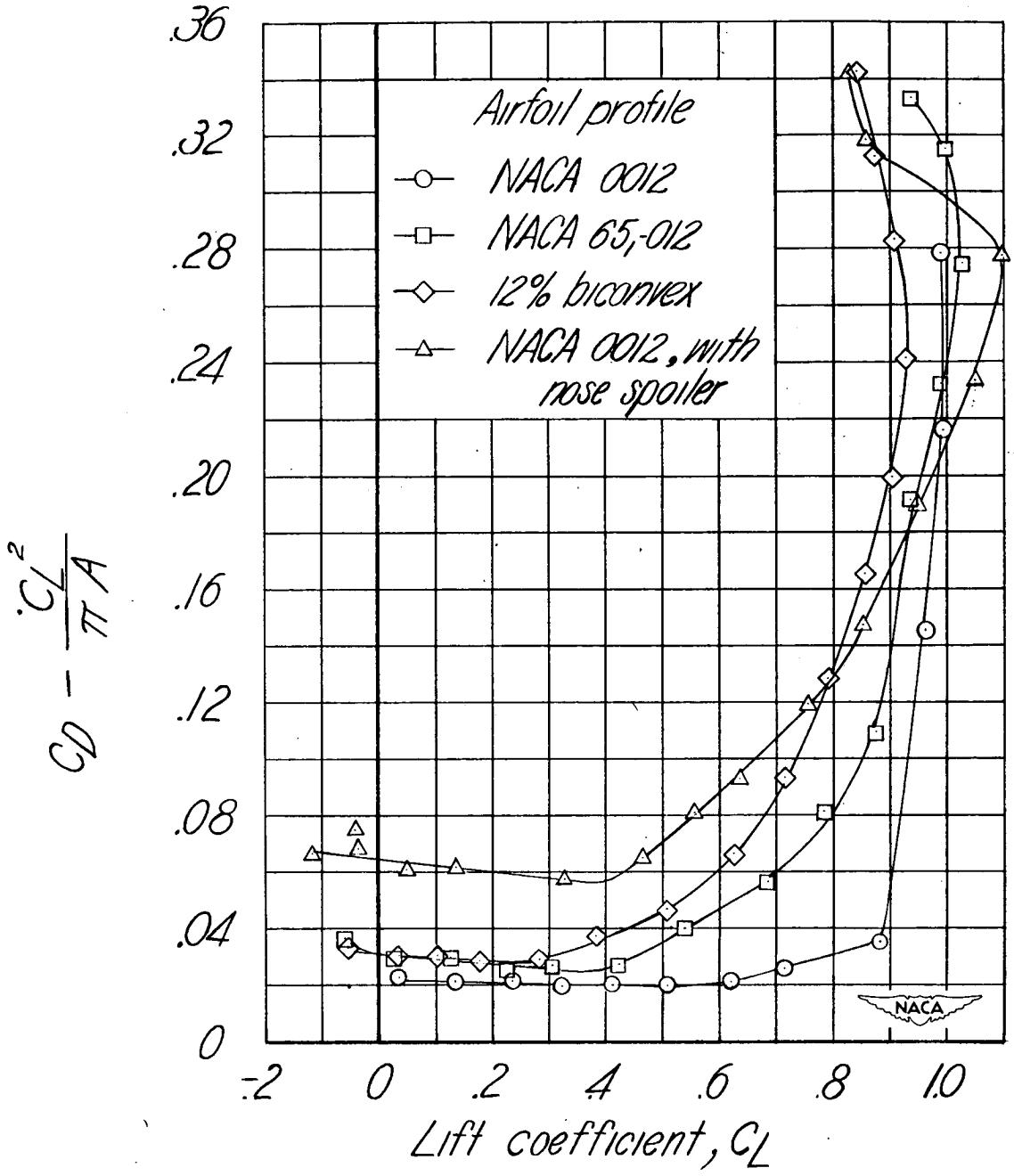

Figure 7.- Variation of the increment in drag $C_D - \frac{C_L^2}{\pi A}$ with lift coefficient for the wings tested.

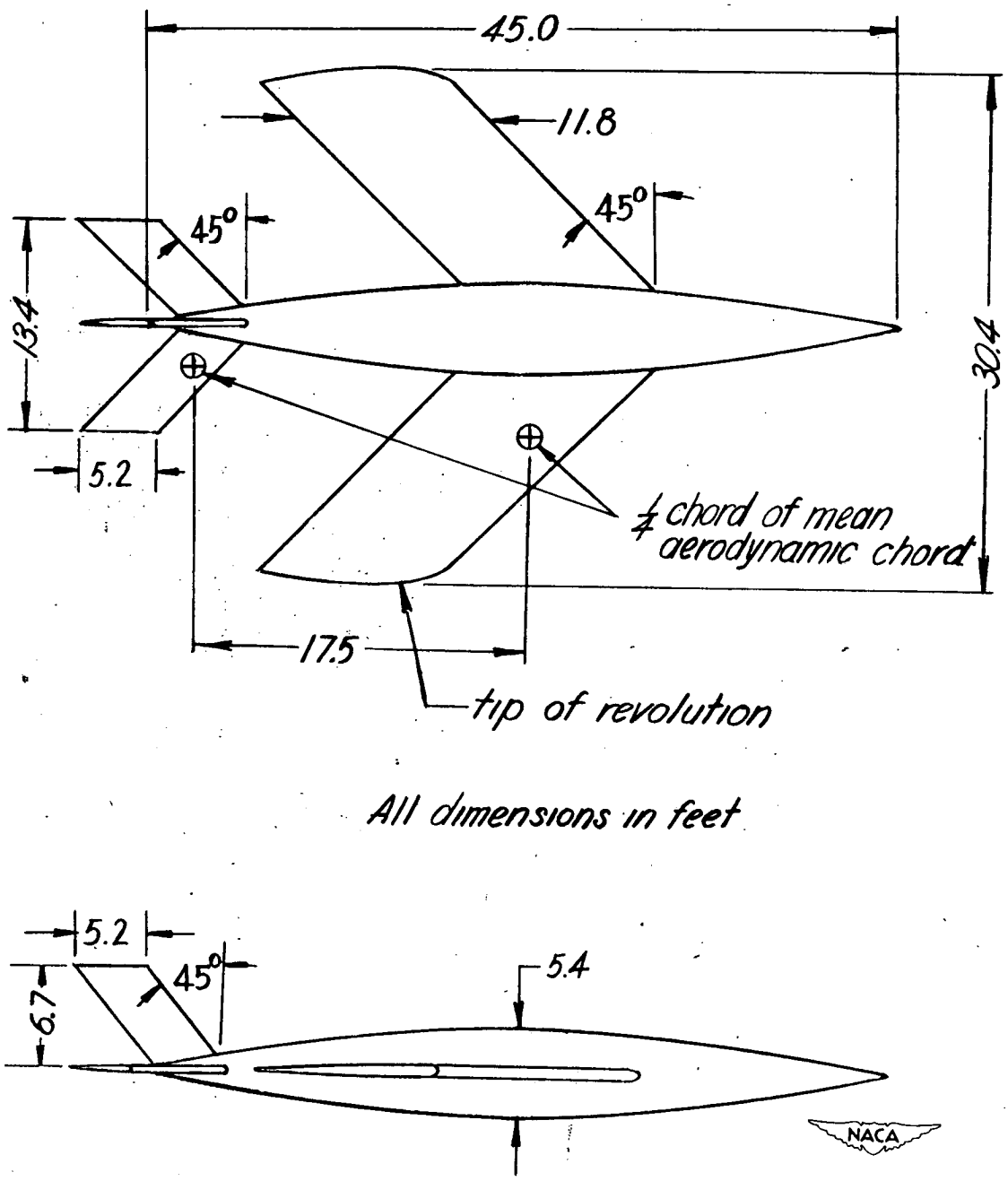

Figure 8.– Sketch of the hypothetical airplane for which stability boundaries and motions were computed.

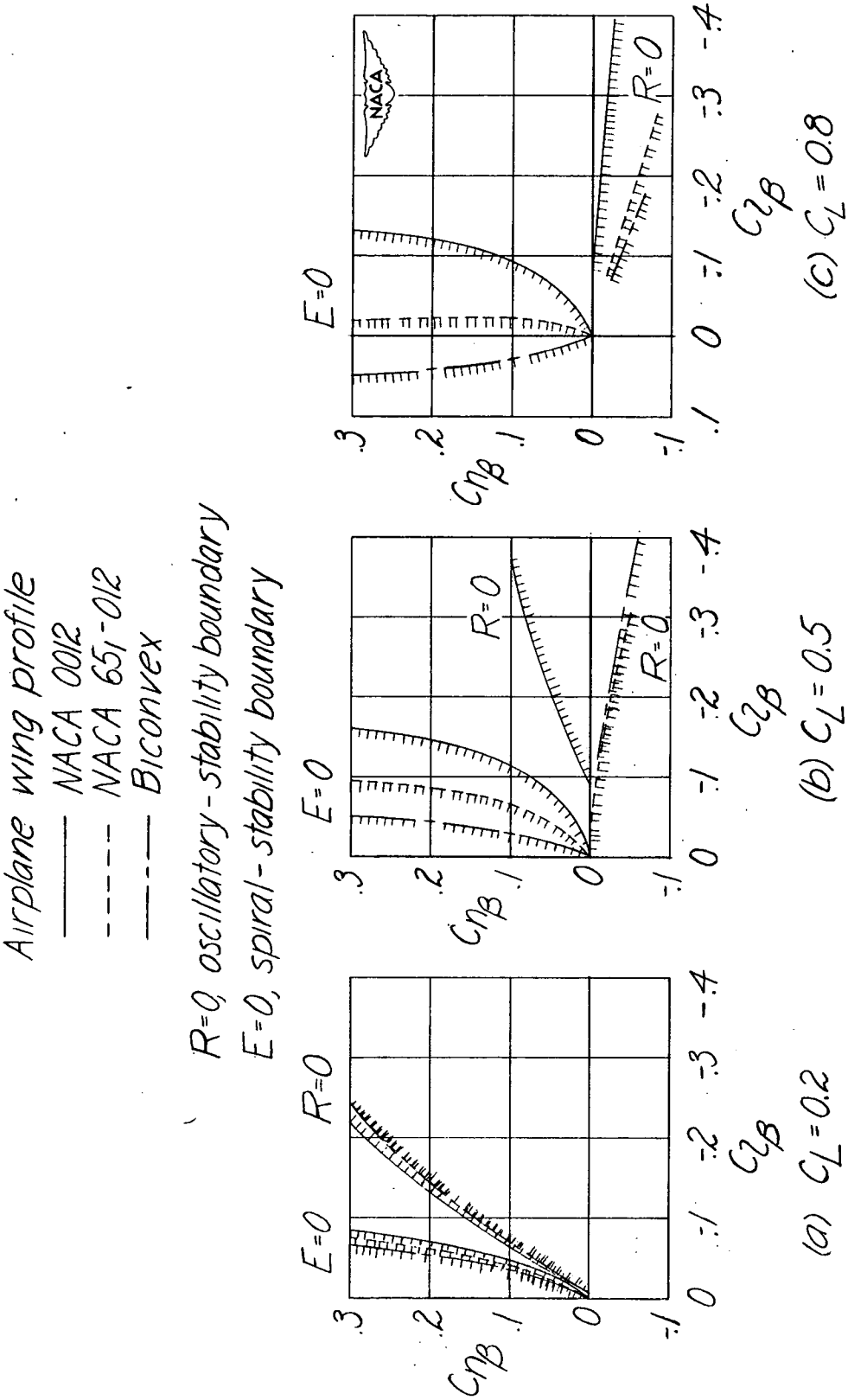

Figure 9.- Lateral stability boundaries for three hypothetical transonic airplanes differing only in wing profile.

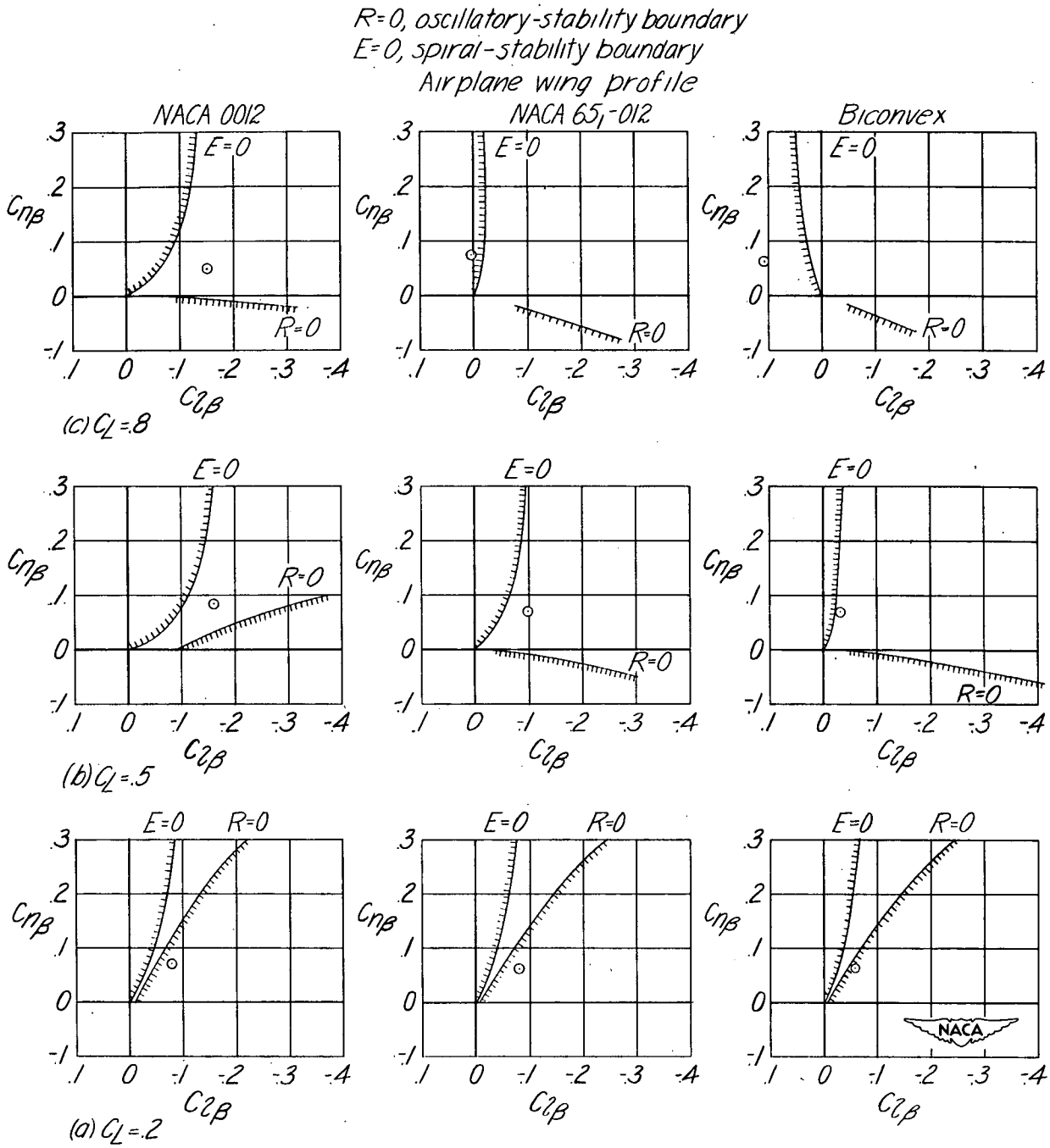

Figure 10.— Lateral stability boundaries for the three hypothetical transonic airplanes showing position of the airplanes with respect to the boundaries.

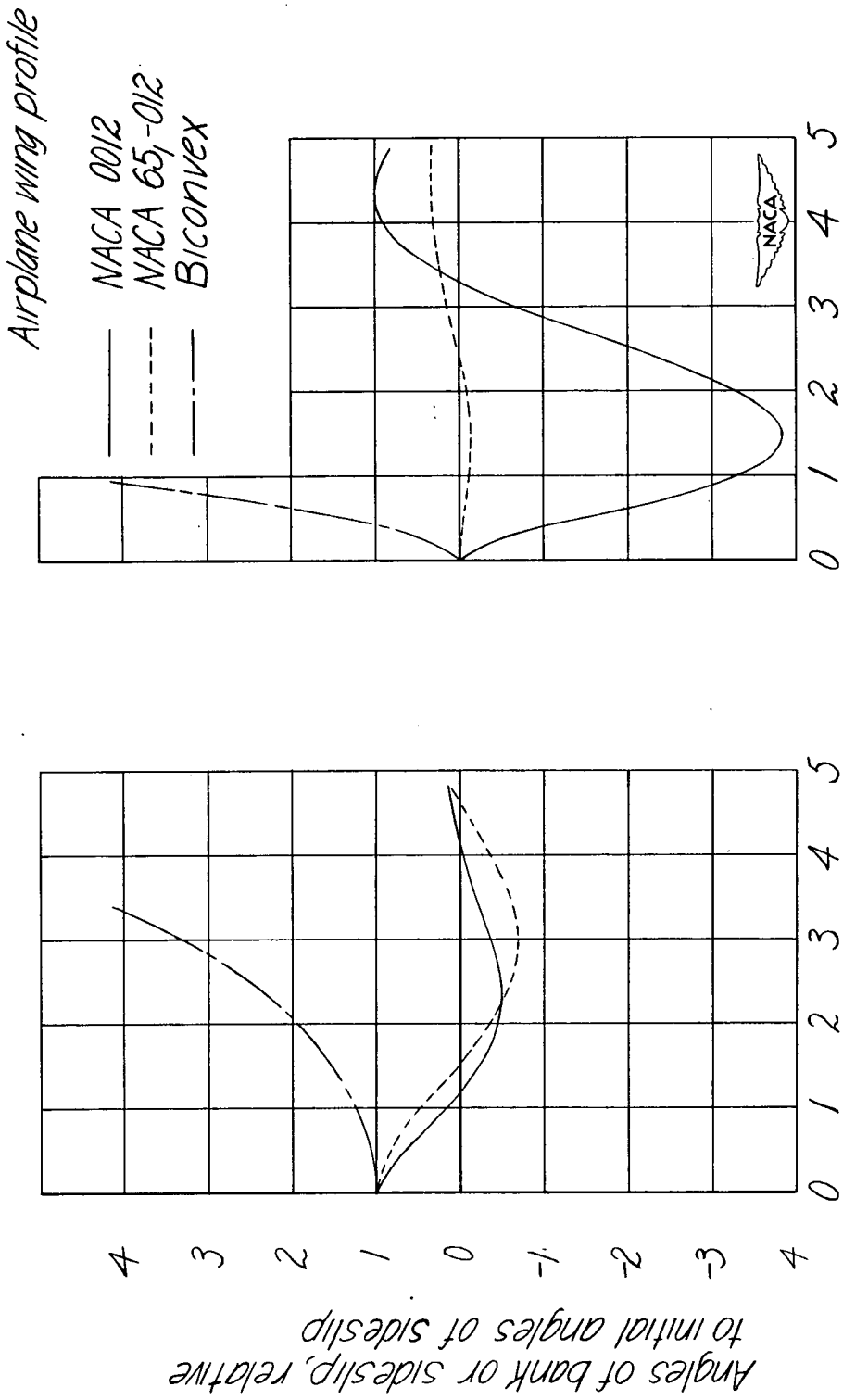

Figure 11.- Motions in bank and sideslip of the three hypothetical transonic airplanes resulting from an initial angle of sideslip. $C_L = 0.8$.